Electronic structure and thermoelectric properties of half-Heusler alloys NiTZ

Cite as: AIP Advances **11**, 025304 (2021); https://doi.org/10.1063/5.0031512
Submitted: 02 October 2020 • Accepted: 02 January 2021 • Published Online: 01 February 2021

Dhurba R. Jaishi, Nileema Sharma, Bishnu Karki, et al.

Electronic structure and thermoelectric properties of half-Heusler alloys NiTZ

Cite as: AIP Advances 11, 025304 (2021); doi: 10.1063/5.0031512
Submitted: 2 October 2020 • Accepted: 2 January 2021 •
Published Online: 2 February 2021

Dhurba R. Jaishi,[1,2] Nileema Sharma,[1,2] Bishnu Karki,[1,2] Bishnu P. Belbase,[1,2] Rajendra P. Adhikari,[3] and Madhav P. Ghimire[1,2,a)]

AFFILIATIONS

[1]Central Department of Physics, Tribhuvan University, Kirtipur 44613, Kathmandu, Nepal
[2]Condensed Matter Physics Research Center (CMPRC), Butwal 32907, Rupandehi, Nepal
[3]Department of Physics, Kathmandu University, Dhulikhel 45200, Nepal

[a)]**Author to whom correspondence should be addressed:** madhav.ghimire@cdp.tu.edu.np

ABSTRACT

We investigated the electronic and thermoelectric properties of half-Heusler alloys NiTZ (T = Sc and Ti; Z = P, As, Sn, and Sb) having an 18 valence electron count. Calculations were performed by means of density functional theory and the Boltzmann transport equation with constant relaxation time approximation, validated by NiTiSn. The chosen half-Heuslers were found to be indirect bandgap semiconductors, and the lattice thermal conductivity was comparable with the state-of-the-art thermoelectric materials. The estimated power factor for NiScP, NiScAs, and NiScSb revealed that their thermoelectric performance can be enhanced by an appropriate doping rate. The value of ZT found for NiScP, NiScAs, and NiScSb is 0.46, 0.35, and 0.29, respectively, at 1200 K.

I. INTRODUCTION

In the past few decades, researchers have been focused on the investigation of multi-functional materials, which can be used in various applications such as in spintronics, optoelectronics, thermoelectrics, and so on. With the surge in demand for green energy sources, TE materials are extensively taken into considerations for their ability to convert relatively small and waste heat into useful energy at the time of energy consumption. A wide range of materials have been explored for potential half-metals and thermoelectric (TE) devices such as organic thermoelectric materials,[1] chalcogenides,[2,3] skutterudites,[4–6] oxides,[7–12] hybrid perovskites,[13–15] triple-point metals,[16] ternary compounds,[17] and half-Heusler (hH) alloys.[18–29] Among them, Heusler compounds have gained much more attention since their discovery in 1903 due to their simple crystalline structure with fascinating properties such as magnetism, half-metallicity, superconductivity, optoelectronics, piezoelectric semiconductors, thermoelectricity, topological insulators, and semimetals.[30–38]

Thermoelectric materials are found to be applicable in day-to-day lives to fulfill the increasing demand of energy of the globalized society. The highly efficient TE devices (cooler, power generator, temperature sensors, and so on) can utilize a large amount of wasted thermal energy to generate electricity and vice versa.[39,40] For this, the device needs a larger figure of merit (ZT), which depends on the transport properties[41,42] defined by

$$ZT = \frac{\alpha^2 \sigma T}{\kappa}, \tag{1}$$

where α (V K^{-1}) is the Seebeck coefficient, σ (S m^{-1}) is the electrical conductivity, $\kappa = \kappa_e + \kappa_l$ (W m^{-1} K^{-1}) is the thermal conductivity, and T(K) is the absolute temperature. $\alpha^2\sigma$ is defined as the power factor (PF). The symbols κ_e and κ_l represent the electronic and lattice thermal conductivity, respectively. The materials having a high value of PF along with the low value of κ are suitable for the efficient TE devices.[43]

Among others, most of the cubic hH alloys with an 18 valence electron count (VEC) exhibits high Seebeck coefficients and are reported as promising materials for TE applications due to high electrical conductivity and narrow bandgap semiconductors with novel electrical and mechanical properties even at high temperatures.[19–22,44] In addition to it, hH alloys contain non-toxic and

readily available elements, making them environmental-friendly and more cost effective.

Recent experimental and theoretical investigations on hH alloys are mainly focused on improving their thermoelectric efficiency ZT by tuning the power factor and thermal conductivity. Bandgap engineering and fluctuation of carrier concentration around the Fermi level (E_F) in the Z position are the widely used methods to enhance the power factor, whereas the thermal conductivity can be decreased by alloying or by doping on the X or Y site to fluctuate the mass of the carriers introducing impurities and nanostructuring.[45–48]

From the literature, we noticed that Ni-based hH alloys with 18 VEC are less investigated. Following Slater–Pauling's rule, the total magnetic moment for these types of hH alloys should be zero. Thus, the zero moment on Ti or Sc at the Y site and P or As or Sb at the Z site will give rise to zero moment for the Ni atom at the X site resulting in a non-magnetic system.[49,50] This motivates us to explore the electronic, TE, and other related properties to confirm if these groups of materials could be suitable for TE devices.

II. COMPUTATIONAL DETAILS

The cubic hH alloys NiTZ (T = Sc and Ti; Z = P, As, Sn, and Sb) belong to the Cl_b structure with space group $F\bar{4}3m$. It contains three in-equivalent atoms forming inter-penetrating fcc sublattices with the Wyckoff positions Ni (1/4, 1/4, 1/4), T (1/2, 1/2, 1/2), and Z (0, 0, 0), respectively, as shown in Fig. 1. The iso-structural NiTiSn is used here to validate our calculations based on the earlier reported results (both theoretical and experimental).

The density functional (DF) calculations have been performed using the full-potential linear augmented plane wave (FP-LAPW) method as implemented in the WIEN2k code.[51] We double checked some parts of our calculations using the plane-wave based pseudopotential Quantum Espresso (QE) package.[52] The standard generalized-gradient approximation (GGA) in the parameterization of Perdew, Burke, and Ernzerhof (PBE)[53] was used in the scalar-relativistic mode. The modified Becke–Johnson (mBJ) potential[54] was further included to check the accuracy of the bandgaps. The self-consistency convergence criteria for charge and energy were set to $10^{-4}e$ and 10^{-5} Ry, respectively.

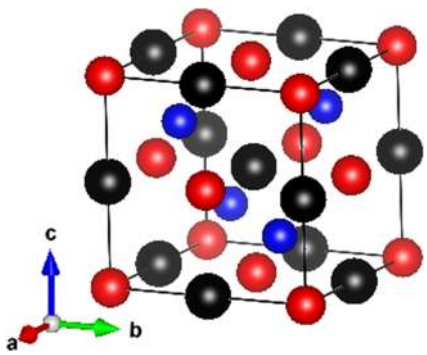

FIG. 1. The crystal structure of cubic hH NiTZ (T = Sc and Ti; Z = P, As, Sn, and Sb). The balls in blue, black, and red color represent Ni, T, and Z atoms, respectively.

In the plane-wave pseudopotential approach, we used the norm-conserving pseudopotentials with plane wave cut-off energy for wave function set to 90 Ry. The full Brillouin Zone (BZ) was sampled with an optimized 10 ×10× 10 mesh of Monkhorst–Pack $k-$points. To check the dynamical stability, phonon spectrum calculations have been performed with a 4 ×4× 4 $q-$ mesh in phonon BZ, which is based on the DF perturbation theory (DFPT) implemented in the QE package.[52]

The TE properties were calculated using the Boltzmann semi-classical transport equation and constant relaxation time approximation based on a smoothed Fourier interpolation of the bands implemented in the BoltzTraP code.[55] The full BZ was sampled with a 50 × 50 × 50$k-$ mesh for the calculation of the transport properties. The electrical conductivity and PF were calculated under constant relaxation time approximation (τ) using the BoltzTraP code based on Boltzmann theory. τ is approximated by fitting the experimental data from the work of Kim *et al.*[18] The lattice thermal conductivity was obtained by solving the linearized Boltzmann transport equation (BTE) within the single-mode relaxation time approximation (SMA) using the thermal2 code implemented in the QE package.[52]

III. RESULTS AND DISCUSSION

A. Structure optimization and phonon stability

We started our calculations by optimizing the cubic hH alloys with $F\bar{4}3m$ symmetry. Our calculated values of lattice parameters and the bandgap within GGA and GGA + mBJ are listed in Table I. These values are found to be in fair agreement with the earlier reports of Ma *et al.*[49] for the GGA case.

The calculated phonon dispersion curves along the high-symmetry points shown in Fig. 2 depict that the proposed hH alloys are thermally stable. This is evidenced by the absence of imaginary phonon frequencies throughout the whole BZ, as expected for dynamic stability.[56] We observed three acoustic (low-frequency region) and six optical phonon (high-frequency region) branches due to three atoms per unit cell. The majority of the lattice contribution to the thermal conductivity arises from the acoustic part as it has high group velocity compared to the optical part. We found that the acoustical phonon branches of NiScP and NiScAs extend nearly to 200 cm^{-1}, while NiScSb and NiTiSn lie within 150 cm^{-1} in frequency. The observation of dynamical stability and preferable energy gap in our proposed hH alloys motivates us to explore the electronic and transport properties for their potential application as TE materials.

TABLE I. The optimized lattice constant a and the bandgap E_g within GGA and GGA + mBJ for the cubic hH alloys NiTZ.

		GGA	GGA+mBJ
System	a (Å)	E_g(eV)	E_g(eV)
NiScP	5.69	0.54	0.62
NiScAs	5.84	0.48	0.52
NiScSb	6.12	0.28	0.32
NiTiSn	5.95	0.46	0.45

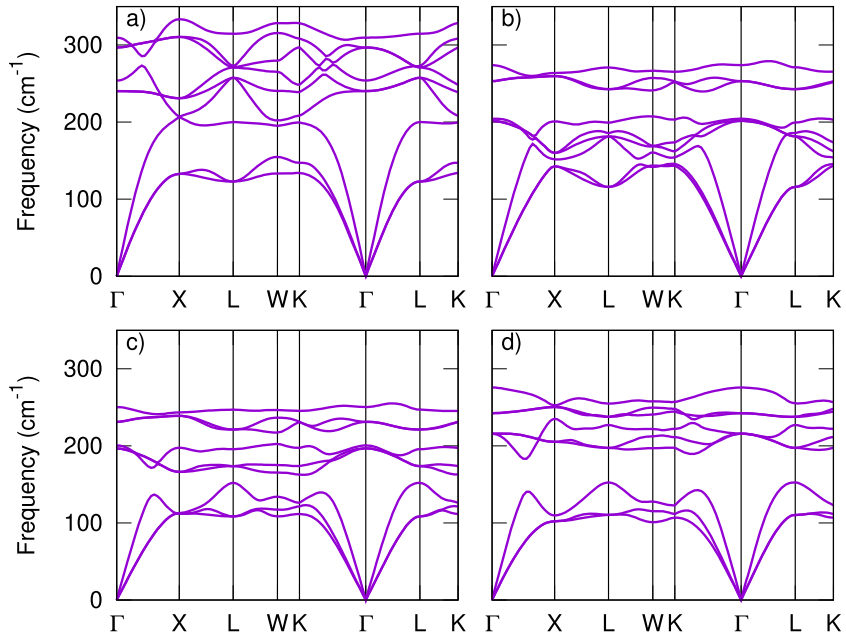

FIG. 2. Phonon band structures for finding the dynamic stability of (a) NiScP, (b) NiScAs, (c) NiScSb, and (d) NiTiSn.

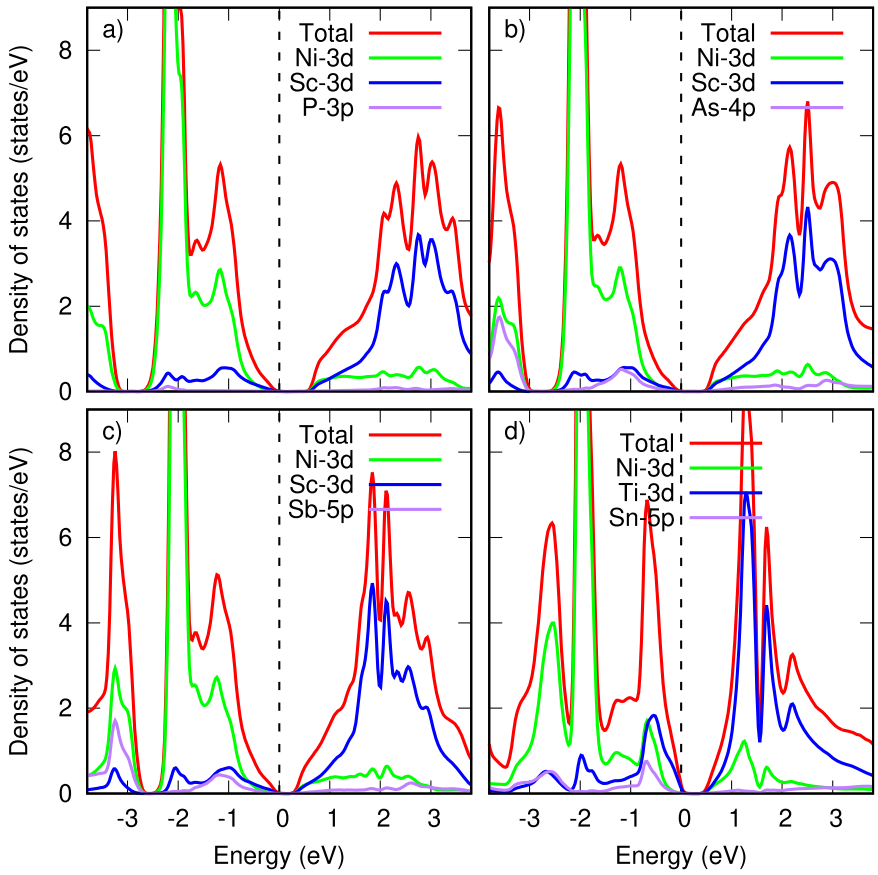

FIG. 3. Total and partial density of states of (a) NiScP, (b) NiScAs, (c) NiScSb, and (d) NiTiSn within GGA + mBJ. The vertical dotted line represents E_F.

B. Electronic properties

To understand the ground state electronic properties of the material, the total and partial density of states (DOS) are shown in Fig. 3. The proposed systems are found to be semiconducting with an energy gap lying within ~ 0.32 eV to 0.62 eV, in fair agreement with the earlier report.[49] As seen in the PDOS, the main contribution to the total DOS at and around E_F is from the 3*d*-orbitals of Ni and Sc atoms, while the contributions from the atom in the Z site are negligible (see Fig. 3). This is an indication that doping onto the Z site may improve the carrier concentration.

It is interesting to note that with an increase in the atomic radius of atoms at the Z site, say, from P to Sb, the bandgap reduces gradually, which further leads to the decrease in the hybridization of Ni-3*d* and Sc-3*d* states. An indirect bandgap is observed in the band structures for hH alloys (see Fig. 4) with their valence band maximum (VBM) lying at Γ and conduction band minimum (CBM) at X in the BZ. The VBM for the hH alloys is threefold degenerate comprising heavy and light bands. From the observed band structure in Fig. 4, the scenario of heavy bands can enhance the Seebeck coefficient, whereas the light band can facilitate the mobility of charge carriers.[57–59] Thus, the combination of heavy and light bands is preferable for increasing the TE performance. The band structure shown in Figs. 4(a)–4(c) dictates the effective mass to be more at $X - \Gamma$ in CBM than that of VBM at Γ (i.e., the effective mass of electron at CBM is greater than that of the hole at VBM), which plays a significant role in TE properties. As seen in NiTiSn [Fig. 4(d)], the VBM (at Γ) is flatter than the CBM (at *X*) indicating that the effective mass of holes at VBM is more than that of electrons on CBM.

C. Transport properties

For an efficient TE material, a high value of α and σ with a low κ is expected, as depicted in Eq. (1). The dimensionless figure of merit *ZT* can be optimized when these parameters are optimum. However, these parameters are inter-related with themselves. Thus, obtaining a high value of *ZT* is in-sufficient just by tuning one or two parameters. To get insight into the TE properties of hH alloys, we calculate the Seebeck coefficient α, electrical conductivity σ/τ, thermal conductivity ($\kappa = \kappa_e + \kappa_l$), power factor (PF), and *ZT* by using constant relaxation time approximation and rigid band approximation.

We first initiate our calculations for NiTiSn by validating the theoretical results, such as PF and thermal conductivity with the reported experimental measurements.[18] From the comparison of the calculated and experimental electrical conductivity, we approximated the relaxation time $\tau = \sim 2 \times 10^{-15}$ s. In the whole process, we use the constant relaxation time, even though it depends on the doping level and temperature, obtained for NiTiSn to implement for all the iso-electronic systems.

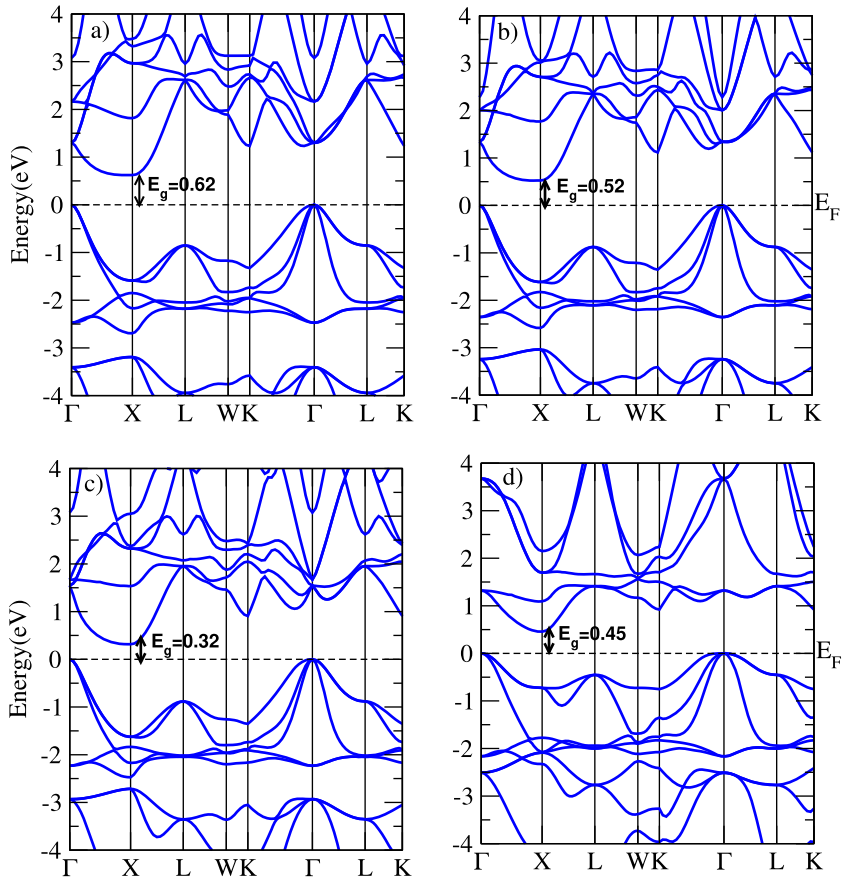

FIG. 4. Electronic band structure of (a) NiScP, (b) NiScAs, (c) NiScSb, and (d) NiTiSn within GGA + mBJ.

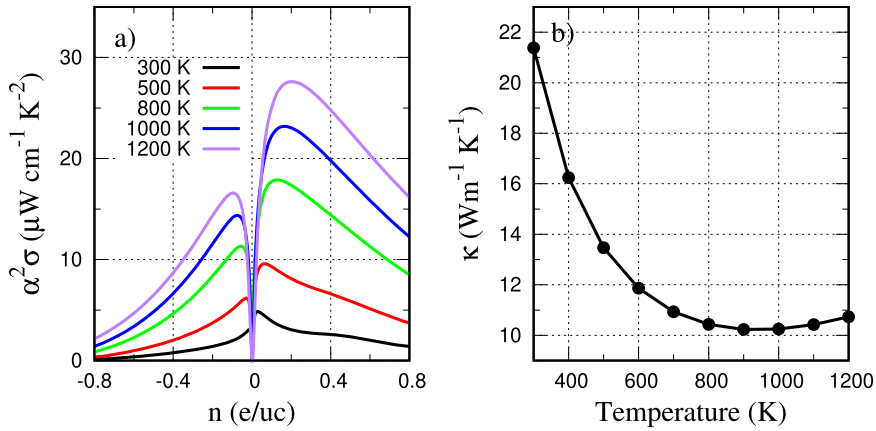

FIG. 5. (a) Power factor as a function of doping level ($e/\mu c$) for NiTiSn. The negative (positive) value represents the electron (hole) doping. (b) Total thermal conductivity as a function of temperature.

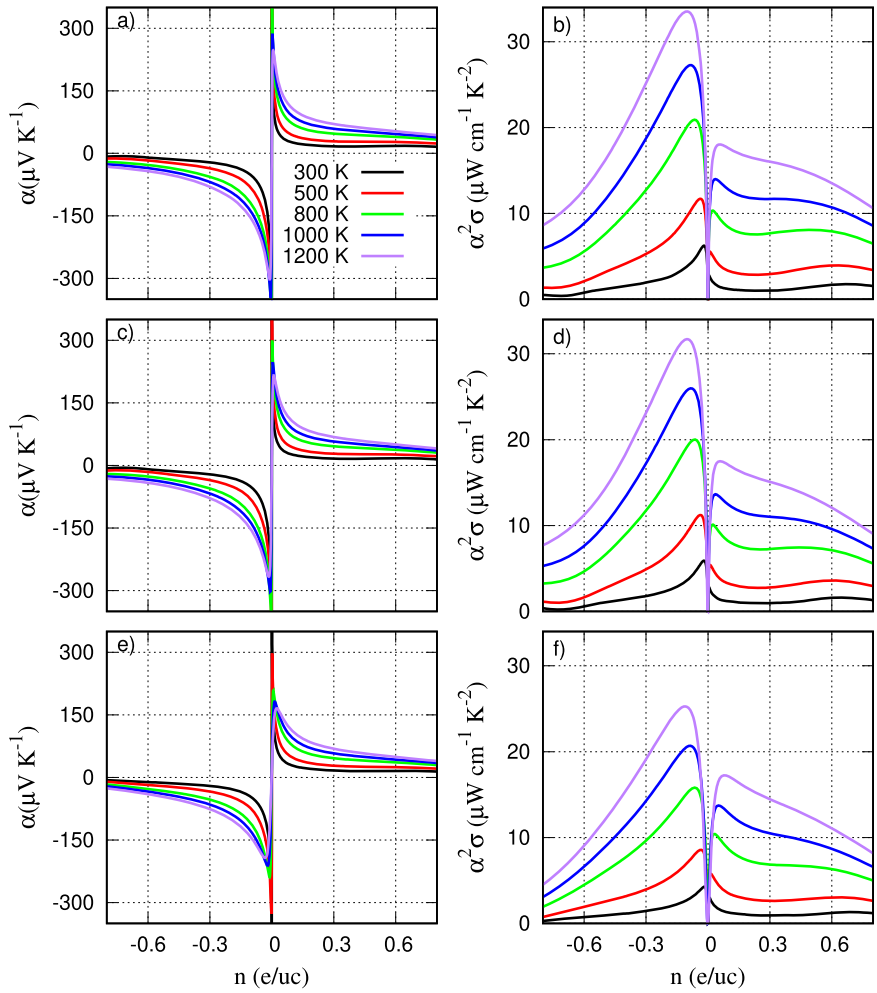

FIG. 6. The Seebeck coefficient [(a), (c), and (e)] and the power factor [(b), (d), and (f)] vs the doping level (in $e/\mu c$) at various temperatures for NiScP, NiScAs, and NiScSb, respectively. The values in negative (positive) values on the horizontal axes represent the electron (hole) doping, respectively.

TABLE II. Calculated optimal doping levels and the corresponding Seebeck coefficient, electrical conductivity, power factor, and *ZT* of NiTZ (T = Sc and Ti; Z = P, As, Sn, and Sb) in cubic symmetry $F\bar{4}3m$ at 1200 K. The negative (−) sign indicates the *n*− type characteristics.

System	n ($e/\mu c$)	α μVK^{-1}	σ ($\times 10^3$ S cm^{-1})	$\alpha^2\sigma$ μW cm^{-1} K^{-2}	ZT
NiTiSn	0.20	154	1.15	27.61	0.30
NiScP	−0.08	−177	1.05	33.16	0.46
NiScAs	−0.08	−168	1.12	31.50	0.35
NiScSb	−0.07	−163	0.90	24.20	0.29

The PF of NiTiSn was reported to be ∼ 16 μW cm^{-1} K^{-2} at 700 K, which upon electron doping (by 1% of the Sb atom to the Sn site) rises to ∼ 30 μW cm^{-1} K^{-2}. When the temperature rises above 700 K, PF is found to decrease in both cases. Comparing these values, we estimate that PF may range between 10 μW cm^{-1} K^{2}and15 μW cm^{-1} K^2 at the 0.04–0.06 doping level of electron per unit cell in the same temperature range. In the case of hole doping, PF lies within 17 μW cm^{-1} K^{-2}–23 μW cm^{-1} K^{-2} at the same temperature range when the dopant is 0.1–0.2 hole per unit cell. This indicates that hole doping is more appropriate than the electrons for PF. The calculated total thermal conductivity 21 Wm^{-1} K^{-1}–10 Wm^{-1} K^{-1} [see Fig. 5(b)] was slightly higher than the earlier report (i.e., 7 Wm^{-1} K^{-1}–10 Wm^{-1} K^{-1}), which is mainly due to the electronic contribution found prominent at higher temperatures. Our calculated results are comparable with the experimental measurements.[18]

The Seebeck coefficient [(a), (c), and (e)] and the PF [(b), (d), and (f)] for different levels of doping are shown in Fig. 6 for NiScP, NiScAs, and NiScSb, respectively. Around E_F (i.e., at μ = 0), the Seebeck coefficient is large (> ±150 μV/K), which on doping to either side falls off significantly. This is evident from its inverse relation with the carrier concentration.

The optimum values of the doping levels and the corresponding TE parameters for 1200 K are listed in Table II.

PF is another parameter to check the reliability of TE materials. As observed in Fig. 6, the PF value for the *p* or *n*− type is significant within the doping range of ±0.3. To be specific, at 1000 K, the calculated values are approximately 15 μW cm^{-1} K^{-2}, 12 μW cm^{-1} K^{-2}, and 13 μW cm^{-1} K^{-2} for NiScP, NiScAs, and NiScSb within 0.02–0.04 hole per unit cell reaching its maximum value at 1200 K. Similarly, for doping range 0.06–0.07 electron per unit cell, PF rises to ∼27 μW cm^{-1} K^{-2}, 25 μW cm^{-1} K^{-2}„ and 20 μW cm^{-1} K^{-2} at 1000 K, respectively. The sizable value of PF within the doping range 0.07–0.08 electron per unit cell suggests that these materials could be good TE materials.

We further show the variation of PF with the chemical potential, μ, in Fig. 7. The peak values of PF noted in the chemical potential range between 0.4 eV and 0.7 eV for NiScP, NiScAs, and NiScSb. In contrast, the peak value of PF is around −0.2 eV for NiTiSn. From the above scenario, electron doping is found to be more suitable for NiScP, NiScAs, and NiScSb due to the larger effective mass of electrons to get a better TE performance. This indicates the presence of larger electron pockets resulting in the dense carriers, which are confined to the CBM along $\Gamma - X$ [Figs. 4(a)–4(c)]. On the other hand, in NiTiSn, hole doping is much more favorable due to the higher effective mass of holes resulting from the nearly flatter band in the VBM and CBM along $\Gamma - X$ [see the band structure in Fig. 4(d)].

Figure 8 shows the calculated thermal conductivity as a function of temperature for NiScP, NiScAs, NiScSb, and NiTiSn, respectively. The total thermal conductivity consists of two components, viz., electronic (κ_e) and lattice (κ_l) parts. At low temperature (say, 300 K), the lattice part was found to be dominant over the electronic part, and with the rise in temperature (say, up to ∼ 900 K, except NiScP), the lattice thermal conductivity and the overall conductivity decrease uniformly.

Note that with an increase in temperature starting from 300 K, the carrier concentration increases resulting in higher electrical conductivity and, hence, the overall thermal conductivity. Similar features were observed in the recent report of CoMnSb.[60] The calculated lattice conductivity is 10.6 Wm^{-1} K^{-1}, 19 Wm^{-1} K^{-1}, and 18.5 Wm^{-1} K^{-1} at 300 K, which reduces abruptly to 2.5 Wm^{-1} K^{-1}, 4.7 Wm^{-1} K^{-1}, and 4.5 Wm^{-1} K^{-1} at 1200 K for NiScP, NiScAs, and NiScSb, respectively.

The figure of merit *ZT* for hH alloys is as shown in Fig. 9. With a low value (say, 0.05) of *ZT* at 300 K, it is found to rise linearly with the increase in temperature. At 1200 K, the calculated values are 0.30, 0.45, 0.35, and 0.29, respectively, for NiTiSn, NiScP, NiScAs,

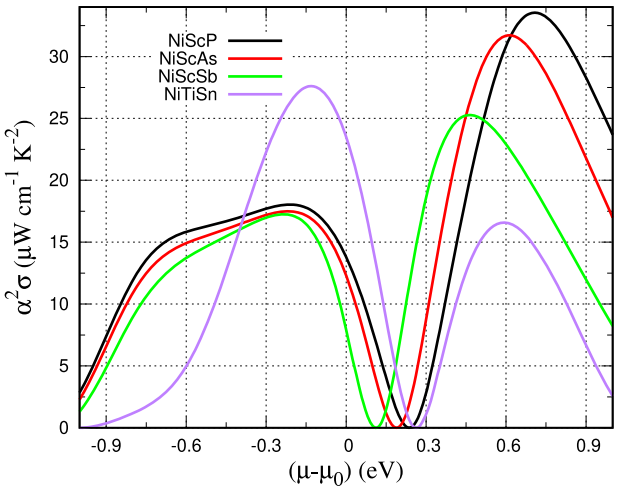

FIG. 7. The power factor vs chemical potential (μ) at 1200 K temperature. The values of chemical potential in negative (positive) represent the hole (electron) doping.

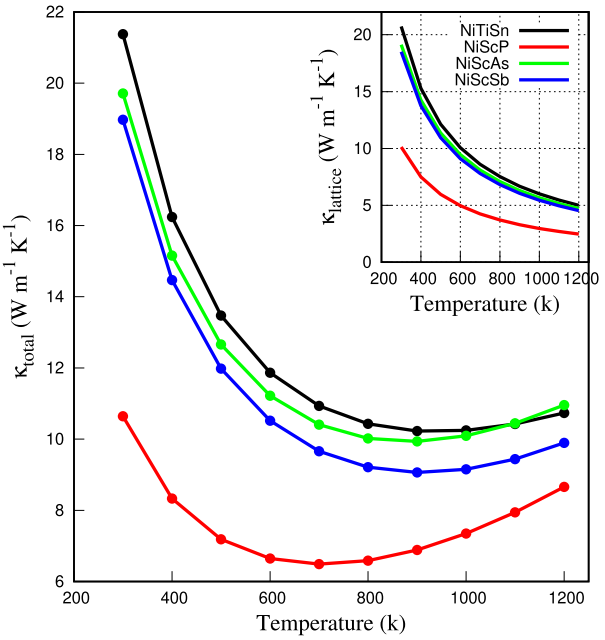

FIG. 8. Total thermal conductivity (κ) as a function of temperature. The inset dictates the lattice contribution to thermal conductivity (κ_l) of NiScP, NiScAs, NiScSb, and NiTiSn.

and NiScSb alloys. On the other hand, the values of total thermal conductivity are found to be minimum at ~ 700 K for NiScP and ~ 900 K for the remaining systems, which start increasing afterward due to the dominance of electronic part. The variation of *ZT* with temperature shows linear nature. PF is dominant at a higher temperature range due to the increase in carrier concentration along with the electrical conductivity. The observed *ZT* is low mainly due to a higher value of κ. Even if our *ZT* values are lower than the commercialized TE materials such as Bi_2Te_3 and PbTe, they can be enhanced by means of doping to any of the three atomic sites. Though the *ZT* value is low (~ 0.05) for the pristine systems compared to the widely used doped Bi-based alloys, say, Bi_2Se_3 (~ 0.01to0.05),[61] Bi_2Se_3 at Bi_2Te_3 (~ 0.7),[62] and Bi–Sb alloys (~ 0.4),[63] it can be enhanced by electron doping.[64]

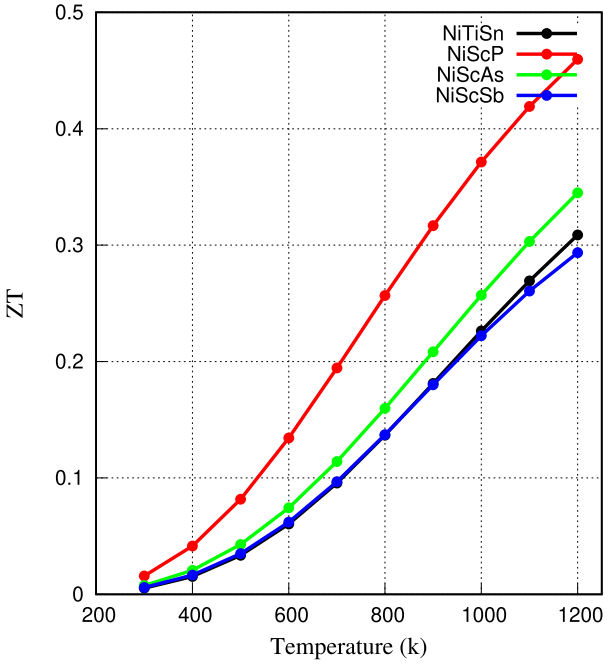

FIG. 9. *ZT* as a function of temperature.

As observed from the calculations above, the *ZT* value can increase when PF is enhanced while minimizing the thermal conductivity. The possible route to tune this from DF is by proper tuning of the bandgap with appropriate electron/hole doping as discussed.

IV. CONCLUSIONS

On the basis of density functional calculations, we investigate the half-Heuslers NiTiSn, NiScP, NiScAs, and NiScSb. Electronic properties reveal that these materials are semiconductors with an indirect bandgap. The narrow bandgap marks them as suitable candidates for TE performance. The calculated power factor shows a large value in both the electron and hole doping cases. Electron doping is found to be more preferable than hole doping for NiScP, NiScAs, and NiScSb, while hole doping is preferable for NiTiSn. Based on the constant relaxation time approximation and rigid band approximation with sizable *ZT*, these compounds are predicted as possible TE materials.

ACKNOWLEDGMENTS

M.P.G. acknowledges the Department of Science and Technology, India, for awarding the India Science and Research Fellowship (ISRF-2019) with Grant No. DO/CCSTDS/201/2019 and the Alexander von Humboldt Foundation, Germany, for the equipment subsidy grants. Part of this work was performed at IIT Roorkee, India, during the ISRF-2019 program, and part of it was performed with the computational resources provided by the Kathmandu University Supercomputer Center established with the equipment donated by CERN. M.P.G. thanks H. C. Kandpal for fruitful discussions suggesting the half-Heusler group to explore and also for all the logistic and technical supports at IIT Roorkee.

There is no conflict of interest.

DATA AVAILABILITY

The data that support the findings of this study are available with the corresponding author and can be obtained upon reasonable request.

REFERENCES

[1] B. Russ, A. Glaudell, J. J. Urban, M. L. Chabinyc, and R. A. Segalman, "Organic thermoelectric materials for energy harvesting and temperature control," Nat. Rev. Mater. **1**, 1–14 (2016).
[2] M. G. Kanatzidis, "Nanostructured thermoelectrics: The new paradigm?," Chem. Mater. **22**, 648–659 (2010).

[3]G. J. Snyder and E. S. Toberer, "Complex thermoelectric materials," in *Materials for Sustainable Energy: A Collection of Peer-Reviewed Research and Review Articles from Nature Publishing Group* (World Scientific, 2011), pp. 101–110.
[4]Y. Lan, A. J. Minnich, G. Chen, and Z. Ren, "Enhancement of thermoelectric figure-of-merit by a bulk nanostructuring approach," Adv. Funct. Mater. **20**, 357–376 (2010).
[5]J. R. Szczech, J. M. Higgins, and S. Jin, "Enhancement of the thermoelectric properties in nanoscale and nanostructured materials," J. Mater. Chem. **21**, 4037–4055 (2011).
[6]A. Shankar, D. P. Rai, M. Ghimire, R. Thapa *et al.*, "Electronic structure and thermoelectricity of filled skutterudite $EuRu_4As_{12}$: A DFT calculation," Indian J. Phys. **91**, 17–23 (2017).
[7]M. P. Ghimire, Sandeep, and R. K. Thapa, "Study of the electronic properties of CrO_2 using density functional theory," Mod. Phys. Lett. B **24**, 2187–2193 (2010).
[8]M. P. Ghimire, R. K. Thapa, D. P. Rai, Sandeep, T. P. Sinha, and X. Hu, "Half metallic ferromagnetism in tri-layered perovskites $Sr_4T_3O_{10}$ (T= Co, Rh)," J. Appl. Phys. **117**, 063903 (2015).
[9]M. P. Ghimire and X. Hu, "Compensated half metallicity in osmium double perovskite driven by doping effects," Mater. Res. Express **3**, 106107 (2016).
[10]P. Roy, V. Waghmare, and T. Maiti, "Environmentally friendly $Ba_xSr_{2-x}TiFeO_6$ double perovskite with enhanced thermopower for high temperature thermoelectric power generation," RSC Adv. **6**, 54636–54643 (2016).
[11]W. S. Choi, H. K. Yoo, and H. Ohta, "Polaron transport and thermoelectric behavior in La-doped $SrTiO_3$ thin films with elemental vacancies," Adv. Funct. Mater. **25**, 799–804 (2015).
[12]S. R. Bhandari, D. K. Yadav, B. P. Belbase, M. Zeeshan, B. Sadhukhan, D. P. Rai, R. K. Thapa, G. C. Kaphle, and M. P. Ghimire, "Electronic, magnetic, optical and thermoelectric properties of $Ca_2Cr_{1-x}Ni_xOsO_6$ double perovskites," RSC Adv. **10**, 16179–16186 (2020).
[13]A. Filippetti, C. Caddeo, P. Delugas, and A. Mattoni, "Appealing perspectives of hybrid lead–iodide perovskites as thermoelectric materials," J. Phys. Chem. C **120**, 28472–28479 (2016).
[14]C. Lee, J. Hong, A. Stroppa, M.-H. Whangbo, and J. H. Shim, "Organic–inorganic hybrid perovskites ABI_3 (A= CH_3NH_3, NH_2CHNH_2; B= Sn, Pb) as potential thermoelectric materials: A density functional evaluation," RSC Adv. **5**, 78701–78707 (2015).
[15]Y. Liu, X. Li, J. Wang, L. Xu, and B. Hu, "An extremely high power factor in Seebeck effects based on a new n-type copper-based organic/inorganic hybrid $C_6H_4NH_2CuBr_2I$ film with metal-like conductivity," J. Mater. Chem. A **5**, 13834–13841 (2017).
[16]S. Singh, Q. Wu, C. Yue, A. H. Romero, and A. A. Soluyanov, "Topological phonons and thermoelectricity in triple-point metals," Phys. Rev. Mater. **2**, 114204 (2018).
[17]D. P. Rai, A. Shankar, A. P. Sakhya, T. Sinha, P. Grima-Gallardo, H. Cabrera, R. Khenata, M. P. Ghimire, R. Thapa *et al.*, "Electronic, optical and thermoelectric properties of bulk and surface (001) cuinte2: A first principles study," J. Alloys Compd. **699**, 1003–1011 (2017).
[18]S.-W. Kim, Y. Kimura, and Y. Mishima, "High temperature thermoelectric properties of TiNiSn-based half-Heusler compounds," Intermetallics **15**, 349–356 (2007).
[19]C. Fu, S. Bai, Y. Liu, Y. Tang, L. Chen, X. Zhao, and T. Zhu, "Realizing high figure of merit in heavy-band p-type half-Heusler thermoelectric materials," Nat. Commun. **6**, 1–7 (2015).
[20]H. Zhu, R. He, J. Mao, Q. Zhu, C. Li, J. Sun, W. Ren, Y. Wang, Z. Liu, Z. Tang *et al.*, "Discovery of ZrCoBi based half Heuslers with high thermoelectric conversion efficiency," Nat. Commun. **9**, 1–9 (2018).
[21]H. Zhu, J. Mao, Y. Li, J. Sun, Y. Wang, Q. Zhu, G. Li, Q. Song, J. Zhou, Y. Fu *et al.*, "Discovery of TaFeSb-based half-Heuslers with high thermoelectric performance," Nat. Commun. **10**, 1–8 (2019).
[22]T. Graf, P. Klaer, J. Barth, B. Balke, H.-J. Elmers, and C. Felser, "Phase separation in the quaternary Heusler compound $CoTi_{(1-x)}Mn_xSb$ a reduction in the thermal conductivity for thermoelectric applications," Scr. Mater. **63**, 1216–1219 (2010).
[23]M.-S. Lee, F. P. Poudeu, and S. D. Mahanti, "Electronic structure and thermoelectric properties of sb-based semiconducting half-Heusler compounds," Phys. Rev. B **83**, 085204 (2011).
[24]M. Zeeshan, T. Nautiyal, J. van den Brink, and H. C. Kandpal, "FeTaSb and FeMnTiSb as promising thermoelectric materials: An *ab initio* approach," Phys. Rev. Mater. **2**, 065407 (2018).
[25]S. Singh, M. Zeeshan, U. Singh, J. van den Brink, and H. C. Kandpal, "First-principles investigations of orthorhombic-cubic phase transition and its effect on thermoelectric properties in cobalt-based ternary alloys," J. Phys.: Condens. Matter **32**, 055505 (2019).
[26]M. Zeeshan, H. K. Singh, J. van den Brink, and H. C. Kandpal, "*Ab initio* design of new cobalt-based half-Heusler materials for thermoelectric applications," Phys. Rev. Mater. **1**, 075407 (2017).
[27]M. Zeeshan, J. van den Brink, and H. C. Kandpal, "Hole-doped cobalt-based Heusler phases as prospective high-performance high-temperature thermoelectrics," Phys. Rev. Mater. **1**, 074401 (2017).
[28]S. Singh, M. Zeeshan, J. v. d. Brink, and H. C. Kandpal, "*Ab initio* study of Bi-based half Heusler alloys as potential thermoelectric prospects," arXiv:1904.02488 (2019).
[29]D. P. Rai, A. Shankar, M. Ghimire, R. Khenata, R. Thapa *et al.*, "Study of the enhanced electronic and thermoelectric (Te) properties of $Zr_xHf_{1-x-y}Ta_yNiSn$: A first principles study," RSC Adv. **5**, 95353–95359 (2015).
[30]S. Sakurada and N. Shutoh, "Effect of ti substitution on the thermoelectric properties of (Zr, Hf)NiSn half-Heusler compounds," Appl. Phys. Lett. **86**, 082105 (2005).
[31]A. Roy, J. W. Bennett, K. M. Rabe, and D. Vanderbilt, "Half-Heusler semiconductors as piezoelectrics," Phys. Rev. Lett. **109**, 037602 (2012).
[32]Z. H. Liu, H. N. Hu, G. D. Liu, Y. T. Cui, M. Zhang, J. L. Chen, G. H. Wu, and G. Xiao, "Electronic structure and ferromagnetism in the martensitic-transformation material Ni_2FeGa," Phys. Rev. B **69**, 134415 (2004).
[33]W. Feng, D. Xiao, Y. Zhang, and Y. Yao, "Half-Heusler topological insulators: A first-principles study with the Tran-Blaha modified Becke-Johnson density functional," Phys. Rev. B **82**, 235121 (2010).
[34]R. A. de Groot, F. M. Mueller, P. G. v. Engen, and K. H. J. Buschow, "New class of materials: Half-metallic ferromagnets," Phys. Rev. Lett. **50**, 2024–2027 (1983).
[35]M. P. Ghimire, Sandeep, T. P. Sinha, and R. K. Thapa, "First principles study of the electronic and magnetic properties of semi-Heusler alloys NiXSb (X= Ti, V, Cr and Mn)," J. Alloys Compd. **509**, 9742–9752 (2011).
[36]Sandeep, M. P. Ghimire, D. Deka, D. P. Rai, A. Shankar, and R. K. Thapa, "Magnetic and electronic properties of half-metallic NiTbSb: A first principles study," Indian J. Phys. **86**, 301–305 (2012).
[37]Y. Nakajima, R. Hu, K. Kirshenbaum, A. Hughes, P. Syers, X. Wang, K. Wang, R. Wang, S. R. Saha, D. Pratt *et al.*, "Topological RPdBi half-Heusler semimetals: A new family of noncentrosymmetric magnetic superconductors," Sci. Adv. **1**, e1500242 (2015).
[38]J. Zhang, J. Chen, P. Li, C. Zhang, Z. Hou, Y. Wen, Q. Zhang, W. Wang, and X. Zhang, "Topological electronic state and anisotropic fermi surface in half-Heusler GdPtBi," J. Phys.: Condens. Matter **32**, 355707 (2020).
[39]V. Zaitsev, M. Fedorov, I. Eremin, E. Gurieva, and D. Rowe, *Thermoelectrics Handbook: Macro to Nano* (CRC Press; Taylor & Francis, Boca Raton, 2006).
[40]S. B. Riffat and X. Ma, "Thermoelectrics: A review of present and potential applications," Appl. Therm. Eng. **23**, 913–935 (2003).
[41]Y. Pei, X. Shi, A. LaLonde, H. Wang, L. Chen, and G. J. Snyder, "Convergence of electronic bands for high performance bulk thermoelectrics," Nature **473**, 66–69 (2011).
[42]A. D. LaLonde, Y. Pei, H. Wang, and G. Jeffrey Snyder, "Lead telluride alloy thermoelectrics," Mater. Today **14**, 526–532 (2011).
[43]J. R. Sootsman, D. Y. Chung, and M. G. Kanatzidis, "New and old concepts in thermoelectric materials," Angew. Chem., Int. Ed. **48**, 8616–8639 (2009).
[44]C. Felser, G. H. Fecher, and B. Balke, "Spintronics: A challenge for materials science and solid-state chemistry," Angew. Chem., Int. Ed. **46**, 668–699 (2007).
[45]J. P. Heremans, V. Jovovic, E. S. Toberer, A. Saramat, K. Kurosaki, A. Charoenphakdee, S. Yamanaka, and G. J. Snyder, "Enhancement of thermoelectric efficiency in PbTe by distortion of the electronic density of states," Science **321**, 554–557 (2008).
[46]L.-D. Zhao, S.-H. Lo, Y. Zhang, H. Sun, G. Tan, C. Uher, C. Wolverton, V. P. Dravid, and M. G. Kanatzidis, "Ultralow thermal conductivity and high thermoelectric figure of merit in snse crystals," Nature **508**, 373–377 (2014).

[47]K. Biswas, J. He, I. D. Blum, C.-I. Wu, T. P. Hogan, D. N. Seidman, V. P. Dravid, and M. G. Kanatzidis, "High-performance bulk thermoelectrics with all-scale hierarchical architectures," Nature **489**, 414–418 (2012).
[48]E. S. Toberer, A. Zevalkink, and G. J. Snyder, "Phonon engineering through crystal chemistry," J. Mater. Chem. **21**, 15843–15852 (2011).
[49]J. Ma, V. I. Hegde, K. Munira, Y. Xie, S. Keshavarz, D. T. Mildebrath, C. Wolverton, A. W. Ghosh, and W. Butler, "Computational investigation of half-Heusler compounds for spintronics applications," Phys. Rev. B **95**, 024411 (2017).
[50]H. C. Kandpal, G. H. Fecher, and C. Felser, "Calculated electronic and magnetic properties of the half-metallic, transition metal based Heusler compounds," J. Phys. D: Appl. Phys. **40**, 1507 (2007).
[51]P. Blaha, K. Schwarz, G. K. Madsen, D. Kvasnicka, J. Luit *et al.*, "wien2k," an augmented plane wave+ local orbitals program for calculating crystal properties, 2001.
[52]P. Giannozzi, S. Baroni, N. Bonini, M. Calandra, R. Car, C. Cavazzoni, D. Ceresoli, G. L. Chiarotti, M. Cococcioni, I. Dabo *et al.*, "QUANTUM ESPRESSO: A modular and open-source software project for quantum simulations of materials," J. Phys.: Condens. Matter **21**, 395502 (2009).
[53]J. P. Perdew, K. Burke, and M. Ernzerhof, "Generalized gradient approximation made simple," Phys. Rev. Lett. **77**, 3865 (1996).
[54]F. Tran and P. Blaha, "Accurate band gaps of semiconductors and insulators with a semilocal exchange-correlation potential," Phys. Rev. Lett. **102**, 226401 (2009).
[55]G. K. H. Madsen and D. J. Singh, "Boltztrap. A code for calculating band-structure dependent quantities," Comput. Phys. Commun. **175**, 67–71 (2006).
[56]A. Togo and I. Tanaka, "First principles phonon calculations in materials science," Scr. Mater. **108**, 1–5 (2015).
[57]C. Kumarasinghe and N. Neophytou, "Band alignment and scattering considerations for enhancing the thermoelectric power factor of complex materials: The case of Co-based half-Heusler alloys," Phys. Rev. B **99**, 195202 (2019).
[58]L. Zhang, M.-H. Du, and D. J. Singh, "Zintl-phase compounds with $SnSb_4$ tetrahedral anions: Electronic structure and thermoelectric properties," Phys. Rev. B **81**, 075117 (2010).
[59]C. Fu, H. Wu, Y. Liu, J. He, X. Zhao, and T. Zhu, "Enhancing the figure of merit of heavy-band thermoelectric materials through hierarchical phonon scattering," Adv. Sci. **3**, 1600035 (2016).
[60]A. Hori, S. Minami, M. Saito, and F. Ishii, "First-principles calculation of lattice thermal conductivity and thermoelectric figure of merit in ferromagnetic half-Heusler alloy CoMnSb," Appl. Phys. Lett. **116**, 242408 (2020).
[61]S. K. Mishra, S. Satpathy, and O. Jepsen, "Electronic structure and thermoelectric properties of bismuth telluride and bismuth selenide," J. Phys.: Condens. Matter **9**, 461 (1997).
[62]Y. Min, J. W. Roh, H. Yang, M. Park, S. I. Kim, S. Hwang, S. M. Lee, K. H. Lee, and U. Jeong, "Surfactant-free scalable synthesis of Bi_2Te_3 and Bi_2Se_3 nanoflakes and enhanced thermoelectric properties of their nanocomposites," Adv. Mater. **25**, 1425–1429 (2013).
[63]B. Lenoir, M. Cassart, J.-P. Michenaud, H. Scherrer, and S. Scherrer, "Transport properties of Bi-rich Bi-Sb alloys," J. Phys. Chem. Solids **57**, 89–99 (1996).
[64]T. Fang, F. Li, Y. Wu, Q. Zhang, X. Zhao, and T. Zhu, "Anisotropic thermoelectric properties of n-type Te-free $(Bi, Sb)_2Se_3$ with orthorhombic structure," ACS Appl. Energy Mater. **3**, 2070–2077 (2020).